

# Equilibrium phase diagram of a randomly pinned glass-former

Misaki Ozawa

*Institute of Physics, University of Tsukuba, Tsukuba 305-8571, Japan  
and Department of Physics, Nagoya University, Nagoya 464-8602, Japan*

Walter Kob

*Laboratoire Charles Coulomb, UMR 5221, University of Montpellier and CNRS, Montpellier, France*

Atsushi Ikeda

*Fukui Institute for Fundamental Chemistry, Kyoto University, Kyoto, 606-8103, Japan*

Kunimasa Miyazaki

*Department of Physics, Nagoya University, Nagoya 464-8602, Japan*

We use computer simulations to study the thermodynamic properties of a glass former in which a fraction  $c$  of the particles has been permanently frozen. By thermodynamic integration, we determine the Kauzmann, or ideal glass transition, temperature  $T_K(c)$  at which the configurational entropy vanishes. This is done without resorting to any kind of extrapolation, *i.e.*,  $T_K(c)$  is indeed an equilibrium property of the system. We also measure the distribution function of the overlap, *i.e.*, the order parameter that signals the glass state. We find that the transition line obtained from the overlap coincides with that obtained from the thermodynamic integration, thus showing that the two approaches give the same transition line. Finally we determine the geometrical properties of the potential energy landscape, notably the  $T$ - and  $c$ -dependence of the saddle index and use these properties to obtain the dynamic transition temperature  $T_d(c)$ . The two temperatures  $T_K(c)$  and  $T_d(c)$  cross at a finite value of  $c$  and indicate the point at which the glass transition line ends. These findings are qualitatively consistent with the scenario proposed by the random first order transition theory.

PACS numbers:

Upon cooling, glass-forming liquids show a dramatic increase of their viscosities and relaxation times before they eventually fall out of equilibrium at low temperatures [1, 2]. This laboratory glass transition is a purely kinetic effect since it occurs at the temperature at which the relaxation time of the system crosses the time scale imposed by the experiment, *e.g.*, via the cooling rate. Despite the intensive theoretical, numerical, and experimental studies of the last five decades, the mechanism responsible for the slowing down and thus for the (kinetic) glass transition is still under debate and hence a topic of intense research. From a fundamental point of view the ultimate goal of these studies is to find an answer to the big question in the field: Does there exist a *finite* temperature at which the dynamics truly freezes and, if it does, whether this *ideal* glass transition is associated with a thermodynamic singularity or whether it is of kinetic origin [3–6].

Support for the existence of a kinetic transition comes from certain lattice gas models with a “facilitated dynamics” [6]. In these models, the dynamics is due to the presence of “defects” and hence for such systems the freezing is not related to any thermodynamic singularity. However, the first evidence that there does indeed exist a thermodynamic singularity goes already back to Kauzmann who found that the residual entropy (the difference of the entropy of the liquid state from that of the crystalline state) vanishes at a finite temperature  $T_K$

if it is extrapolated to temperatures below the laboratory glass transition [7]. Subsequently many theoretical scenarios that invoke the presence of a thermodynamic transition have been proposed [8–10]. One of these is the so-called “random first order transition” (RFOT) theory which, inspired by the exact solution of a mean-field spin glass, predicts that at  $T_K$  the glass-former does indeed undergo a thermodynamic transition at which the residual, or configurational entropy  $S_c$  (the logarithm of the number of the states which are available to the system) vanishes and concomitantly breaks the replica symmetry [10, 11]. A further appealing feature of RFOT is that it seems to reconcile in a natural way the (free) energy-landscape scenario and mode-coupling theory (MCT), a highly successful theory that describes the relaxation dynamics at intermediate temperatures [12].

Despite all these advances, the arguments put forward in the various papers must be considered as phenomenological since compelling and undisputed experimental or numerical evidence to prove or disprove any of these theories and scenarios is still lacking. The only exception are hard spheres in infinite dimensions, for which mean-field theory should become exact [13], but even in this case some unexpected problems are present, see Ref. [14]. This lack of understanding is mainly due to the steep increase of the relaxation times which hampers the access to the transition point of thermally equilibrated systems and hence most of the efforts to identifying the transition

point, if it exists, resort on unreliable extrapolation.

## I. RANDOMLY PINNED SYSTEMS

Recently a novel idea to bypass this difficulty has been proposed [15–18]. By freezing, or pinning, a fraction of the degrees of freedom of the system, the ideal glass transition temperature has been predicted to rise to a point at which experiments and simulations *in equilibrium* are feasible thus allowing to probe the nature of this transition. In Ref. [15] the authors have studied the effect of pinning for the case of a mean-field spin glass model which is known to exhibit a dynamical MCT-transition at a temperature  $T_d$  and a thermodynamic transition at a lower temperature  $T_K$ . It was demonstrated that, by pinning a fraction  $c$  of the degree of freedoms of the spins (selected at random) in the equilibrated system, both  $T_K(c)$  and  $T_d(c)$  increase with  $c$ . Thus by equilibrating the non-pinned system at an intermediate temperature and subsequently increasing  $c$ , one can access and probe the ideal glass state in *thermal equilibrium* (Note that changing  $c$  does not perturb this equilibrium [19]). It was found that at sufficiently large  $c$  the two lines  $T_K(c)$  and  $T_d(c)$  merge and terminate at a critical point with a universality class of the random-field Ising model [15, 20].

Very recently, it has been tested whether this approach to detect  $T_K$  in mean field models can also be used in realistic glass formers in finite dimensions [21]. It was found that pinned systems do indeed show a behavior that agrees qualitatively with the theoretical predictions, thus giving encouraging evidence that the nature of the ideal glass transition can be studied in equilibrium. In these numerical studies, the overlap  $q$  and its distribution  $[P(q)]$  have been used to identify the amorphous-fluid phase diagram in the  $T$ - $c$  plane for pinned systems [21].

Despite these results, it is not clear if the so obtained amorphous state is the *bona fide* ideal glass, for which the configurational entropy  $S_c$  vanishes and, in view of the conceptual importance of  $S_c$ , this is a very disturbing situation. We recall that  $S_c$  is related to the number of available states of the system [10, 11] and is also a key quantity that controls the slow dynamics in the activation regime in which the relaxation time  $\tau_\alpha$  is related to  $S_c$  via the Adam-Gibbs relation,  $\ln \tau_\alpha \propto 1/T S_c$  [10, 22]. Finally,  $S_c$  is intimately related to the Landau-like free energy associated to the overlap of two coupled replicas [23].

Although from the simulations reported in Ref. [21], the existence of  $T_K$  has been inferred from the behavior of the overlap distribution  $[P(q)]$  (discussed in more detail below), such an analysis of the overlap  $q$  alone may not be conclusive to demonstrate the existence of the arrested phase, since one can not exclude the possibility that other scenarios, such as the purely kinetic one, can also explain the observed features of  $[P(q)]$ . Thus, evaluating  $S_c$  directly and identifying the temperature at which it vanishes is crucial to disentangle conflicting theoretical scenarios.

In the present work, we use computer simulation to determine for a canonical glass-former with pinned particles the ideal glass transition temperature  $T_K(c)$  as a point at which  $S_c$  vanishes. For the first time this is done without invoking any kind of extrapolation. We also calculate the overlap distribution  $[P(q)]$  and find that  $T_K$  obtained from  $S_c(T_K) = 0$  and from  $[P(q)]$  agree very well up to a finite value of  $c$ . Furthermore, we analyze the geometrical properties of the potential energy landscape (PEL) and use it to evaluate the dynamic transition temperature  $T_d(c)$  as a point at which the saddles of the energy landscape vanish. We find that  $T_d(c)$  merges with  $T_K(c)$  exactly at the point at which the two mentioned  $T_K(c)$  depart from each other, strongly indicating the existence of a critical point which is predicted by the mean-field analysis [15–17].

## II. RESULTS

We study a standard glass-forming model: A three dimensional binary Lennard-Jones mixture [24]. The number of particles is  $N = 150$  and  $300$ , but most of the results are for  $N = 300$  (see *Materials and Methods* for details). Throughout the present study, the system has been prepared at each temperature by randomly choosing a fraction  $c$  of particles from the thermally equilibrated samples and quenching their positions (see *Materials and Methods* for details).

### A. Entropy and configurational entropy

To obtain the entropy of the pinned system,  $S$ , we used thermodynamic integration to determine the entropy of a given configuration of pinned particles and subsequently calculated  $S$  by averaging over the realizations of pinned particles (see *Materials and Methods* for details).

Figure 1(a) shows the entropy per (unpinned) particle  $s \equiv S/N(1 - c)$  as a function of the fraction of pinned particles at several temperatures  $T$  and we recognize that with increasing  $c$  the entropy decreases rapidly. For all temperatures this decrease is linear at small  $c$  but then the curves bend at intermediate  $c$  and follow a weaker  $c$ -dependence. For  $T \lesssim 0.5$  this bent becomes sharp, strongly indicating that a *thermodynamic* glass transition takes place.

This becomes more evident by evaluating the configurational entropy obtained by subtracting from  $S$  the vibrational entropy  $S_{\text{vib}}$ . In order to estimate  $S_{\text{vib}}$ , we have determined the inherent structures [25] and calculated the eigenfrequencies  $\omega_a$ . Using the harmonic approximation, one can then approximate  $S_{\text{vib}} = \sum_a \{1 - \log(\beta \hbar \omega_a)\}$ .  $s_{\text{vib}} \equiv S_{\text{vib}}/N(1 - c)$  is shown in Fig. 1(a) as well (solid lines) and we see that it shows basically a linear decrease with  $c$ , a trend which is due to the suppression of the low frequency modes in the density of states.

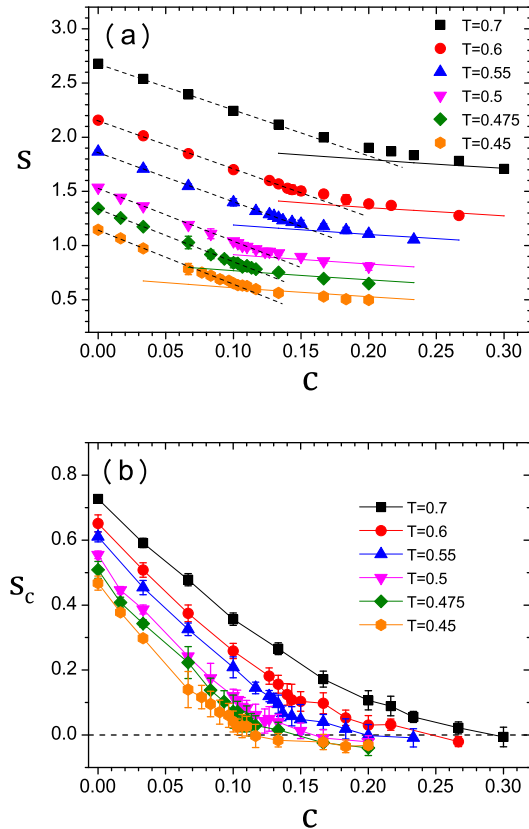


FIG. 1: (a): Entropy of the system,  $s$ , as evaluated from the thermodynamic integration, as a function of  $c$  (symbols). The entropies of the disordered solid states  $s_{\text{vib}}$ , obtained using the harmonic approximation, are drawn as solid lines. The dashed lines are a linear extrapolation from the low  $c$  sides. (b): The configurational entropy  $s_c = s - s_{\text{vib}}$ . The error bars have been estimated from the sample to sample fluctuations.

We can now estimate the configurational entropy  $S_c$  as the difference  $S_c = S - S_{\text{vib}}$  [26] and in Fig. 1(b) we show the  $c$ -dependence of  $s_c = S_c/N(1 - c)$  for various temperatures. This figure shows that, for  $T \lesssim 0.5$ ,  $s_c$  quickly decreases with increasing  $c$  and becomes basically zero at a finite value of  $c$ , indicating that the system has entered the ideal glass state in which the entropy is basically due to harmonic vibrations [27]. For  $T \gtrsim 0.55$ , the approach of  $s_c$  to zero is milder and the bent is less sharp, indicating that the transition becomes a crossover.

We define the ideal glass transition point  $c_K(T)$ , or  $T_K(c)$ , as the point at which  $s_c$  becomes zero. As the temperature is lowered,  $c_K(T)$  decreases and in Fig. 4 we show the resulting phase diagram the details of which will be discussed below. Finally we mention that the presented results are for  $N = 300$ . However, we have also simulated systems with  $N = 150$  and found that the results do not depend significantly on  $N$  (see SI for details).

## B. Overlap approach

An alternative method to locate and characterize the thermodynamic transition is to study the overlap  $q_{\alpha\beta}$  between two configurations  $\alpha$  and  $\beta$ :  $q_{\alpha\beta} = N^{-1} \sum_{i,j} \theta(a - |\mathbf{r}_i^\alpha - \mathbf{r}_j^\beta|)$ , where  $\theta$  is the Heaviside function,  $\mathbf{r}_i^\alpha$  is the position of particle  $i$  in configuration  $\alpha$ , and the length-scale  $a$  is 0.3 [21]. RFOT predicts that at the glass transition the average value  $[\langle q \rangle]$  will increase quickly from a small value in the fluid phase to a large value in the glass phase [16]. Here  $\langle \dots \rangle$  and  $[\dots]$  stand for the thermal and disorder averages, respectively. We have computed the overlap distribution  $P(q)$  using replica exchange molecular dynamics [21] (see SI) and in Fig. 2 we present  $[P(q)]$  for  $T = 0.7$  and  $0.45$ . For  $T = 0.7$ ,  $[P(q)]$  remains single-peaked for all  $c$ , and the peak position shifts continuously towards larger  $q$  as  $c$  increases, see Fig. 2(a). A qualitatively different behavior is observed at  $T = 0.45$  (Fig. 2(b)):  $[P(q)]$  is single-peaked at low and high  $c$ , but has a double peak structure at intermediate  $c$ , thus signalling the coexistence of the fluid and glass phase, which indicates that the transition from the fluid phase to the glass phase is first-order-like [21].

The  $c$ -dependence of the average overlap  $[\langle q \rangle]$  is shown in Fig. 2(c). For high temperatures  $T \gtrsim 0.6$ ,  $[\langle q \rangle]$  smoothly increases with  $c$ , reflecting the continuous shift of the single peak of  $[P(q)]$  as shown in Fig. 2(a). For  $T \lesssim 0.5$ ,  $[\langle q \rangle]$  shows a quick increase at intermediate values of  $c$ , in agreement with the presence of the double peak structure seen in  $[P(q)]$  at these  $T$ . It suggests that a first-order-like transition, rounded by finite size effect, takes place, in qualitative agreement with the result for a system of harmonic spheres [21]. Note that, within the accuracy of our data, we see that the amplitude of the (smeared out) jump in  $[\langle q \rangle]$  seems to vanish around  $0.55 \lesssim T \lesssim 0.6$ , thus indicating that at around that temperature the line of first order transition ends in a critical point that is second-order-like.

From this approach with the overlap, we can define the ideal glass transition temperature  $T_K^{(q)}(c)$  as the temperature at which the skewness of  $[P(q)]$  vanishes (see SI), and in Fig. 4 we have included the resulting  $T_K^{(q)}(c)$  as well. For small and intermediate  $c$ , we find a very good agreement between  $T_K(c)$  and  $T_K^{(q)}(c)$ , thus showing that the two very different approaches do give the same ideal glass transition temperature. This is thus very strong evidence that at this temperature the system does indeed undergo a thermodynamic phase transition from the fluid to an ideal glass state. For temperatures above the second-order-like critical point the curves  $T_K(c)$  and  $T_K^{(q)}(c)$  differ. We will rationalize this in the Discussion below. Finally we mention that the curves  $T_K(c)$  and  $T_K^{(q)}(c)$  seem to extrapolate in a smooth manner to the Kauzmann temperature of the bulk which has been estimated from extrapolation [26]. This shows that the present measurement of the bulk  $T_K$  is compatible with

the one from previous estimates.

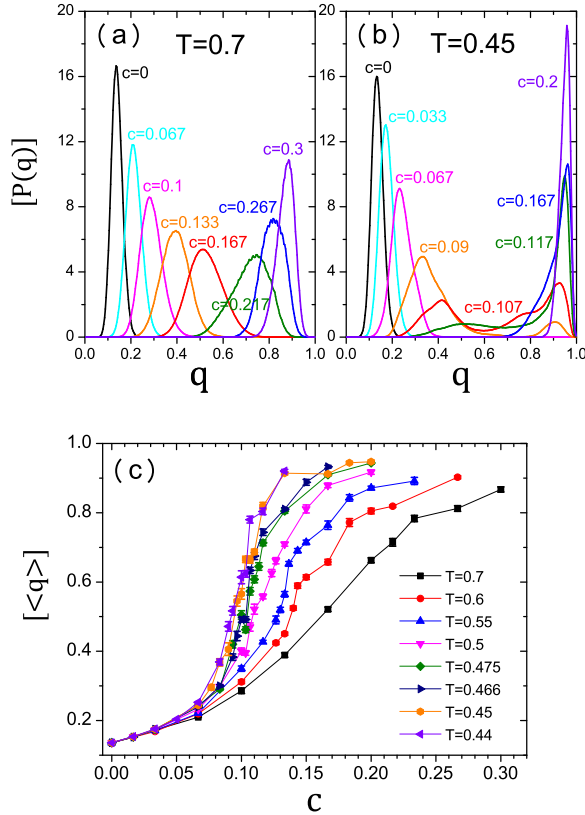


FIG. 2: Distribution of the overlap  $[P(q)]$  for  $T = 0.7$  (a) and  $T = 0.45$  (b). (c): The average overlap  $[\langle q \rangle]$  obtained from  $[P(q)]$  as a function of  $c$  for several temperatures. The error bars have been calculated using the jackknife method.

### C. Potential energy landscape and mode coupling temperature

In the past, it has been found that the slow dynamics of glass-forming systems is closely related to the features of the potential energy landscape (PEL) [29] and in the following we will use these relations to characterize the relaxation dynamics of the pinned system.

Figure 3(a) shows the  $T$ -dependence of the average inherent structure energy  $[\langle e_{IS} \rangle]$ . For the bulk system,  $c = 0$ ,  $[\langle e_{IS} \rangle]$  is basically constant at high temperatures but then steeply decreases below a crossover temperature  $T \approx 1$ , a temperature which signals that the relaxation dynamics becomes strongly influenced by the PEL [30, 31]. As  $c$  increases, the value of  $[\langle e_{IS} \rangle]$  at high  $T$  moves steadily upward, which is reasonable since the energy of the system is literally *pinned* at the higher energy levels due to the presence of the pinned particles. Concomitantly the crossover temperature increases with  $c$  and the crossover becomes smeared out, completely

disappearing at the highest  $c$ . The vanishing of this crossover with growing  $c$  indicates thus that the pinning affects qualitatively the nature of the PEL and of the relaxation dynamics. For instance it is found that with increasing  $c$  the fragility of the system decreases and shows at high  $c$  an Arrhenius dependence [21, 32].

In the inset of Figure 3(a), the low temperature behavior of  $[\langle e_{IS} \rangle]$  is shown. It clearly demonstrates that  $[\langle e_{IS} \rangle]$  is inversely proportional to  $T$  for all  $c$ . According to the energy landscape scenario, this is an indicator that the distribution of  $e_{IS}$  is Gaussian [33].

Another important quantity that connects the glassy dynamics of a system with its PEL is the saddle index  $K$ , *i.e.*, the number of negative eigenvalues of the Hessian matrix at a stationary point of the PEL. For bulk systems it has been found that  $K$  shows a linear dependence on  $e_{SP}$ , the bare energy of a saddle point [34, 35]. Since the value of  $e_{SP}$  at which  $K$  goes to zero (this value is often denoted as “threshold energy”  $e_{th}$ ) corresponds to the average energy of the inherent structures  $\langle e_{IS} \rangle$  at the critical temperature of mode-coupling theory, one can extract from the geometrical properties of the PEL the value of  $T_d$  without having to do any fit to dynamical data [34, 35].

We use a standard method to determine numerically the energy and index of saddles for the pinned system (see SI for details), and in Fig. 3(b) we plot the average normalized saddle index  $k = K/3N(1 - c)$  as a function of its corresponding  $e_{SP}$ . In agreement with previous studies of the PEL, we find that  $k$  decreases linearly as a function of  $e_{SP}$  and hence we can obtain  $e_{th}(c)$  from a linear fit (included in the figure as well). We see immediately that  $e_{th}$  increases with  $c$  and together with the data of Fig. 3(a) and  $e_{th}(c) = [\langle e_{IS} \rangle](T_d(c))$ , we can conclude that  $T_d(c)$  increases with  $c$ . The resulting  $c$ -dependence of  $T_d$  is included in Fig. 4 as well and will be discussed in the next section.

We have also evaluated  $T_d$  by calculating the relaxation time  $\tau_\alpha$  from the time dependent density correlation function (see *Material and Methods*) and by fitting  $\tau_\alpha$  with the MCT power-law  $\tau_\alpha \simeq |T - T_d^{(fit)}|^{-\gamma}$ . We find that the so obtained values of  $T_d^{(fit)}$  agree well with those obtained from the PEL (see SI for details). Note that one needs several fit parameters to obtain  $T_d^{(fit)}$  from the dynamic data, whereas basically no fit parameter are required for  $T_d$  from the PEL. In Fig. 4, the iso- $\tau_\alpha$  lines are also plotted. The graph shows that  $\tau_\alpha$  quickly increases with  $c$  and that the lines asymptotically approach the  $T_K$  line from the high  $T$ -side.

## III. DISCUSSION

In Fig. 4 we summarize the results of the previous sections in the form of a phase diagram in the  $c$ - $T$  plane. The ideal glass transition lines  $T_K(c)$  determined from  $S_c = 0$  and  $T_K^{(q)}(c)$  obtained from  $P(q)$  are plot-



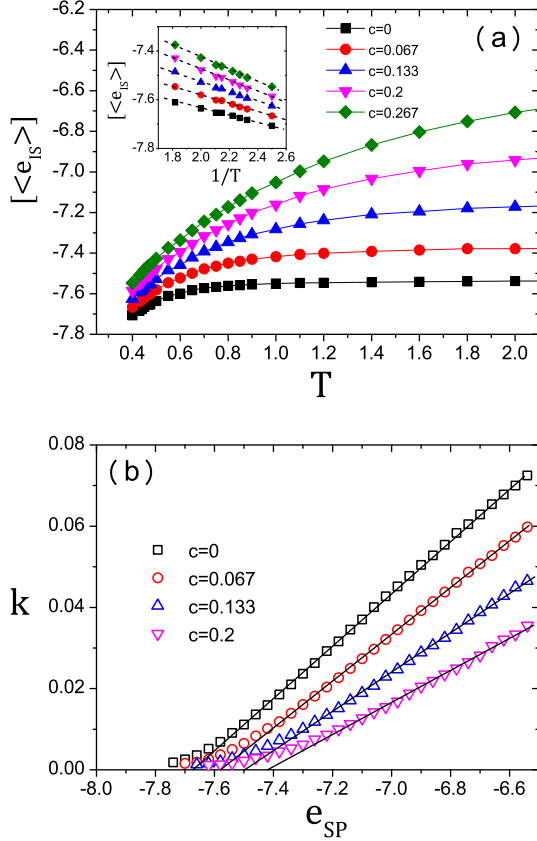


FIG. 3: (a):  $T$  dependence of the averaged inherent structure  $[\langle e_{IS} \rangle]$  for several values of  $c$ . Inset: Same quantity as a function of  $1/T$ . (b): The average normalized saddle index,  $k$ , as a function of its energy,  $e_{SP}$ , for several values of  $c$ . The threshold energy,  $e_{th}$ , is defined by a linear extrapolation from the high energy side.

ted as filled circles and diamonds, respectively. At low  $T$  and  $c$  the two temperatures basically coincide but around  $(T_c, c_c) \approx (0.55, 0.16)$ , they start to depart from each other in that  $T_K^{(q)}(c)$  increases continuously whereas  $T_K(c)$  bends and its  $c$ -dependence becomes weaker. Note that this separation occurs at the same point at which  $[P(q)]$  changes from the bimodal to the single-peaked shape (see Fig. 2), thus indicating that in this region of parameter space the system has a second order like critical point.

The theoretical calculations for a mean-field spin glass model show that  $T_K(c)$  should terminate at a finite  $c$  and that this end point is a critical point of the universality class of the random field Ising model [15–17, 20]. Furthermore the theory predicts that at this end point the coexistence line  $T_K(c)$  and the dynamical line  $T_d(c)$  merge. Figure 4 shows that this prediction is indeed compatible with our data in that the two lines do cross near  $(T_c, c_c)$ .

From the figure we also recognize that, beyond the

endpoint,  $T_K(c)$  obtained from  $S_c = 0$  almost matches with  $T_d(c)$ . This result is reasonable since in this range of  $T$  and  $c$  the particles are strongly confined by the labyrinthine structure imposed by the pinned particles, *i.e.*, the system resides mainly at the bottom of a free energy minimum where both the configurational entropy and the number of the saddles vanish simultaneously. In contrast to  $T_K(c)$ ,  $T_K^{(q)}(c)$  raises continuously even beyond the endpoint. This can be understood by recalling that this line is defined by the points at which the skewness becomes zero, *i.e.*, the point at which  $[P(q)]$  changes from being left-skewed to right-skewed. Since this change of sign in the skewness occurs also in the region of the phase diagram beyond the critical point, the line  $T_K^{(q)}$  will extend into that region, similar to the Widom line present in a standard liquid-gas transition [36, 37].

As it is evident from Fig. 1(a),  $T_K$  defined as the point at which  $S_c = S - S_{vib} = 0$  becomes somewhat ill-defined beyond the endpoint ( $T \gtrsim 0.55$  in Fig. 1(a)), since the crossover from the fluid to the glass phase becomes broad. In order to estimate the effect of this ambiguity, we have included in Fig. 4 also  $T'_K$  defined by the linear extrapolation  $S_c$  of Fig. 1(b) from the *low*  $c$  side (open circles). We see that below the end point  $T \lesssim 0.5$ ,  $T'_K$  is indistinguishable from  $T_K$  whereas beyond the end point  $T \gtrsim 0.6$  they bifurcate and  $T'_K$  becomes comparable with  $T_K^{(q)}$ .

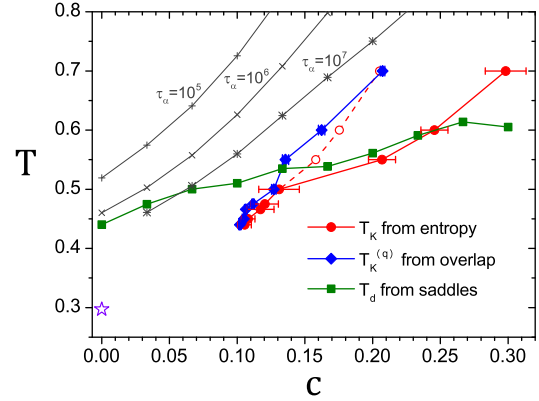


FIG. 4: The phase diagram of the randomly pinned system. The filled circles show the ideal glass line  $T_K$  at which the configurational entropy vanishes. The diamonds show  $T_K^{(q)}(c)$  determined from the skewness of  $[P(q)]$ . The squares are dynamic transition points  $T_d(c)$ . The open circles show the ideal glass line  $T'_K$  determined by the linear extrapolation of  $S_c(c)$  to vanish from Fig. 1(b). The iso-relaxation-times are drawn by  $+$ ,  $\times$ , and  $*$ . The star denoted at  $c = 0$  is a putative ideal glass transition point  $T_K \approx 0.3$  for the bulk reported in Ref. [26].

To the best of our knowledge, the present study is the first report of a system in finite dimensions that shows the existence of an ideal glass state *in equilibrium*, *i.e.*, a state in which the configurational entropy is zero at a finite

$T$ . The Kauzmann temperatures reported in the past have all relied on somewhat questionable extrapolation procedures, leaving thus room for debate over the very existence of a thermodynamic transition [6, 8, 38].

Our findings are inconsistent with recent simulation studies in which the  $T$ - and  $c$ -dependence of the relaxation dynamics has been studied [39]. In Ref. [39], the structural relaxation time  $\tau_\alpha$  was fitted with the Vogel-Fulcher relation  $\tau_\alpha \sim \exp[A/(T - T_0)]$ , with  $T_0$  as fit parameter. This relation can be directly derived from the Adam-Gibbs as well as the RFOT theory, both of which assert that  $\ln \tau_\alpha \propto 1/TS_c$ , and thus the Vogel-Fulcher temperature  $T_0$  is predicted to be identical to  $T_K$ . Furthermore the authors of Ref. [39] fitted their data also with the MCT power-law  $\tau_\alpha \simeq |T - T_d|^{-\gamma}$  in order to determine the  $c$ -dependence of  $T_d$ . It was found that while  $T_d$  increases moderately with  $c$ ,  $T_0$  remains constant. We have plotted the relaxation time  $\tau_\alpha$  as a function of  $S_c$  for finite  $c$  and found that the Adam-Gibbs relation is violated (see SI for details). Thus we conclude that in the case of pinned systems one cannot deduce the Vogel-Fulcher law from the Adam-Gibbs relation.

Since the results presented here are all obtained in thermodynamic equilibrium without referring to any kind of extrapolation, we are confident that the phase diagram presented in Fig. 4 does indeed reflect the properties of the system and is not an artifact of the analysis. A further evidence that the simulated system is really in equilibrium is the observation that the entropy obtained by thermodynamic integration from the high temperature limit matches with that obtained from the low temperature side (via harmonic approximation) in the glass phase. It is also reassuring that all three methods, the thermodynamic integration (vanishing entropy), the overlap distribution (the discontinuous jump of  $q$ ), and the geometric change of the PEL, consistently point to the same end point, thus giving strong evidence that this point really exists. Also suggestive is that each combination of pairs amongst three methods are compatible beyond the end point, which is reminiscent of the Widom line in the standard gas-liquid phase transition.

At this stage we can conclude that the phase diagram as predicted by the RFOT theory is confirmed at least qualitatively. What remains to be done is to probe the relaxation dynamics in the vicinity of the critical end point since one can expect that this dynamics is rather unusual [40] and to establish its universality class [20, 41]. Furthermore, it will also be important to see whether the predicted phase diagram can also be observed in real experiments. Although this will be not easy, for certain systems such as colloids or granular media it should be possible.

## IV. MATERIALS AND METHODS

### A. Model

The system we use is a binary mixture of Lennard-Jones particles [24]. Both species  $A$  and  $B$  have the same mass and the composition ratio is  $N_A : N_B = 80 : 20$ . The interaction potential between two particles is given by  $v_{\alpha\beta}(r) = 4\epsilon_{\alpha\beta}\{(r/\sigma_{\alpha\beta})^{12} - (r/\sigma_{\alpha\beta})^6\}$ , where  $\alpha, \beta \in \{A, B\}$ . We set  $\epsilon_{AA} = 1.0, \epsilon_{AB} = 1.5, \epsilon_{BB} = 0.5, \sigma_{AA} = 1.0, \sigma_{AB} = 0.8$  and  $\sigma_{BB} = 0.88$ .  $v_{\alpha\beta}(r)$  is truncated and shifted at  $r = 2.5\sigma_{\alpha\beta}$ . We show energy in units of  $\epsilon_{AA}$ , with the Boltzmann constant  $k_B = 1$ , and length in units of  $\sigma_{AA}$ . Time units are defined by Monte Carlo sweeps (see below). Simulations are performed at constant density  $\rho \approx 1.2$ . The number of particles is  $N = 150$  and  $300$ , and most of the results in the present study are for  $N = 300$ .

### B. Making pinned configurations

The configuration of the pinned particles is generated by making first a replica exchange run for the bulk system, *i.e.*,  $c = 0$ , using 8 replicas [42]. This allows us to generate relatively quickly many equilibrium configurations that are completely independent, *i.e.*, between consecutive configurations the mean squared displacement of a tagged particle is more than 100. Next we use a “template” to identify the  $cN$  particles that will be permanently pinned. Details on how to create the template can be found in Ref. [21]. This approach has the advantage that the pinned particles cover the space in a relatively uniform manner, thus avoiding the creation of dense regions or large empty regions and hence suppressing strong sample-to-sample fluctuations of the thermodynamic properties of the system.

### C. Simulation methods

- Thermodynamics: In order to sample thermodynamic properties efficiently at low  $T$  and large  $c$  region, we use the replica exchange method [42]. The maximum number of replicas is 24. More detail is presented in the supplemental information and in Ref. [21]. The total CPU time to obtain the presented results is about 580 years of single core time.

- Dynamics: We use the Monte Carlo (MC) dynamics simulation to calculate dynamical observables [43]. The rule of the MC dynamics is the following: In an elementary move, one of the  $(1 - c)N$  unpinned particle is chosen at random. Then the particle is displaced at random within a cubic box of linear size  $\delta = 0.15$  and the standard Metropolis rule is used to decide whether or not the move is accepted. One MC step consists of  $(1 - c)N$  such attempts and we set this as a unit of time scale. The relaxation time  $\tau_\alpha$  is determined by  $F^A(k, \tau_\alpha) = e^{-1}$ ,

where  $F_s^A(k, t)$  is the self part of the intermediate scattering function of the free particles of species  $A$  for the wave-vector  $k$  at the peak of the corresponding structure factor. We have averaged over 30 different realizations of pinned particles to calculate  $F^A(k, t)$ .

#### D. Entropy

In order to calculate the entropy  $S(c, T)$  of the pinned system, we have first determined the entropy of the system for a given configuration of pinned particles, and then taken the average over the realization of the configuration of pinned particles. For this we have calculated the potential energy at temperatures ranging from the target temperature up to the ideal gas limit at  $T = \infty$ , while keeping the pinning configuration fixed. We have evaluated the entropy of the system with that pinning configuration using thermodynamic integration. For this integration, we have used a grid in the inverse temperature  $\beta = 1/T$  of width  $\Delta\beta$  that ranged between 0.01 to 0.1, depending on the temperature, and integrated the potential energy as a function of  $\beta$ . Special care was taken in the very high temperature regime, in order to accurately and rapidly achieve the convergence to high temperature ideal gas limit. The high temperature expansion of the potential energy of Lennard-Jones fluid can be written as  $U = A\beta^{-1/4} + B\beta^{-2/4} + C\beta^{-3/4}$  [44]. We have used simulations at very high temperatures to determine the coefficients  $A$ ,  $B$ , and  $C$ , and carried out then the thermodynamic integration analytically.

#### E. Analysis of the saddles

To locate the saddles of the potential energy landscape of the system, we have made a minimization of the squared gradient potential  $W = \frac{1}{2}|\nabla U|^2$  [34, 35]. Minimization of  $W$  is performed by the BFGS method [45]. Similar to the minimization of  $U$  used to calculate the inherent structures,  $W$  includes the position of the pinned as well as unpinned particles, but only the position of the latter are optimized. After having located a saddle with energy  $e_{\text{SP}}$ , the Hessian matrix was diagonalized and we counted the fraction of negative eigenvalues  $k(e_{\text{SP}})$ . The raw data is shown in the SI and in Fig. 3 (b) we present the average index as a function of  $e_{\text{SP}}$ . The threshold energy  $e_{\text{th}}$  is defined by  $k(e_{\text{th}}) = 0$ .

#### Acknowledgments

We thank G. Biroli, C. Cammarota, D. Coslovich, and K. Kim for helpful discussions. MO acknowledge the financial support by Grant-in-Aid for JSPS Fellows (26.1878). WK acknowledges the Institut Universitaire de France. AI acknowledges JSPS KAKENHI No. 26887021. KM and MO acknowledge KAKENHI No. 24340098, 25103005, 25000002, and the JSPS Core-to-Core Program. The simulations have been done in Research Center for Computational Science, Okazaki, Japan, at the HPC@LR, and the CINES (grant c2014097308).

- 
- [1] P. G. Debenedetti and F. H. Stillinger, Supercooled liquids and the glass transition, *Nature*, **410**, 259 (2001).
  - [2] K. Binder and W. Kob, *Glassy materials and disordered solids* (World Scientific, Singapore, 2011).
  - [3] A. Cavagna, Supercooled liquids for pedestrians, *Phys. Rep.*, **476**, 51 (2009).
  - [4] L. Berthier, G. Biroli, J.-P. Bouchaud, L. Cipelletti, and W. van Saarloos, *Dynamical Heterogeneities in Glasses, Colloids, and Granular Media*, Oxford University Press, Oxford, (2011).
  - [5] L. Berthier and G. Biroli, Theoretical perspective on the glass transition and amorphous materials. *Rev. Mod. Phys.* **83**, 587 (2011).
  - [6] D. Chandler and J. P. Garrahan, Dynamics on the way to forming glass: Bubbles in space-time, *Annual Review of Physical Chemistry*, **61**, 191 (2010).
  - [7] W. Kauzmann, The nature of the glassy state and the behavior of liquids at low temperatures, *Chem. Rev.*, **43**, 219 (1948).
  - [8] G. Tarjus, An overview of the theories of the glass transition. In "Dynamical heterogeneities in glasses, colloids, and granular media", Eds.: L. Berthier, G. Biroli, J.-P. Bouchaud, L. Cipelletti, and W. van Saarloos (Oxford University Press, Oxford, 2011).
  - [9] H. Tanaka, Roles of bond orientational ordering in glass transition and crystallization, *J. Phys.: Condens. Matter*, **23**, 284115 (2011).
  - [10] G. Biroli and J.-P. Bouchaud, The random first-order transition theory of glasses: a critical assessment, In P. G. Wolynes and V. Lubchenko, Eds., *Structural Glasses and Supercooled Liquids: Theory, Experiment, and Applications* (Wiley, New York, 2012).
  - [11] T. R. Kirkpatrick, D. Thirumalai, and P. G. Wolynes, Scaling concepts for the dynamics of viscous liquids near an ideal glassy state, *Phys. Rev. A*, **40**, 1045 (1989).
  - [12] W. Götze, "Complex Dynamics of Glass-Forming Liquids", (Oxford University Press, Oxford, 2009).
  - [13] J. Kurchan, G. Parisi, P. Urbani, and F. Zamponi, Exact Theory of Dense Amorphous Hard Spheres in High Dimension. II. The High Density Regime and the Gardner Transition, *J. Phys. Chem. B*, **117**, 12979 (2013).
  - [14] A. Ikeda and K. Miyazaki Mode-Coupling Theory as a Mean-Field Description of the Glass Transition, *Phys. Rev. Lett.* **104**, 255704 (2010).
  - [15] C. Cammarota and G. Biroli, Ideal glass transitions by random pinning, *Proc. Nat. Acad. Sci. USA*, **109**, 8850 (2012).
  - [16] C. Cammarota and G. Biroli, Random pinning glass transition: Hallmarks, mean-field theory and renormalization group analysis, *J. Chem. Phys.*, **138**, 12A547 (2013).

- [17] C. Cammarota, A general approach to systems with randomly pinned particles: Unfolding and clarifying the random pinning glass transition, *EPL*, **101**, 56001 (2013).
- [18] L. Berthier and W. Kob, Static point-to-set correlations in glass-forming liquids, *Phys. Rev. E*, **85**, 011102 (2012).
- [19] P. Scheidler, W. Kob, and K. Binder, The relaxation dynamics of a supercooled liquid confined by rough walls. *J. Phys. Chem. B*, **108**, 6673 (2004).
- [20] S. Franz and G. Parisi, Universality classes of critical points in constrained glasses, *J. Stat. Mech.*, P11012 (2013).
- [21] W. Kob and L. Berthier, Probing a liquid to glass transition in equilibrium, *Phys. Rev. Lett.*, **110**, 245702 (2013).
- [22] G. Adam and J. H. Gibbs, On the temperature dependence of cooperative relaxation properties in glass-forming liquids, *J. Chem. Phys.*, **43**, 139 (1965).
- [23] S. Franz and G. Parisi, Phase diagram of coupled glassy systems: A mean-field study. *Phys. Rev. Lett.*, **79**, 2486 (1997).
- [24] W. Kob and H. C. Andersen, Testing mode-coupling theory for a supercooled binary Lennard-Jones mixture I: The van Hove correlation function, *Phys. Rev. E*, **51**, 4626 (1995).
- [25] F. H. Stillinger and T. A. Weber, Hidden structure in liquids, *Phys. Rev. A*, **25**, 978 (1982).
- [26] F. Sciortino, W. Kob, and P. Tartaglia, Inherent structure entropy of supercooled liquids, *Phys. Rev. Lett.* **83**, 3214 (1999).
- [27] The fact that the difference  $s - s_{\text{vib}}$  is slightly negative is related to the harmonic approximation used to estimate  $s_{\text{vib}}$ . We have estimated the anharmonic correction to  $s_{\text{vib}}$ , by considering the nonlinear contribution of the potential energy at the inherent structures [29] and found that the corrections are very small and *negative*. Evaluation of the exact values of this correction is, however, difficult and beyond the scope of the present work. In principle one can avoid this difficulty by evaluating the configurational entropy directly [28]. However, at present such an approach is computationally way too expensive for systems close to the ideal glass transition.
- [28] L. Berthier and D. Coslovich, Novel approach to numerical measurements of the configurational entropy in supercooled liquids, *Proc. Nat. Acad. Sci. USA*, **111**, 11668 (2014).
- [29] F. Sciortino, Potential energy landscape description of supercooled liquids and glasses, *J. Stat. Mech.*, P05015 (2005).
- [30] S. Sastry, P. G. Debenedetti, and F. H. Stillinger, Signatures of distinct dynamical regimes in the energy landscape of a glass-forming liquid, *Nature*, **393**, 554 (1998).
- [31] Y. Brumer and D. R. Reichman, Mean-field theory, mode-coupling theory, and the onset temperature in supercooled liquids, *Phys. Rev. E*, **69**, 041202 (2004).
- [32] K. Kim, K. Miyazaki, and S. Saito, Slow dynamics, dynamic heterogeneities, and fragility of supercooled liquids confined in random media, *J. Phys.: Condens. Matter*, **23**, 234123, (2011).
- [33] G. Ruocco, F. Sciortino, F. Zamponi, C. De Michele, and T. Scopigno, Landscapes and fragilities, *J. Chem. Phys.*, **120**, 10666 (2004).
- [34] L. Angelani, R. Di Leonardo, G. Ruocco, A. Scala, and F. Sciortino, Saddles in the energy landscape probed by supercooled liquids, *Phys. Rev. Lett.*, **85**, 5356 (2000).
- [35] K. Broderix, K. K. Bhattacharya, A. Cavagna, A. Zipfelius, and I. Giardina, Energy landscape of a Lennard-Jones liquid: Statistics of stationary points, *Phys. Rev. Lett.*, **85**, 5360 (2000).
- [36] B. Widom, Equation of state in the neighborhood of the critical point, *J. Chem. Phys.*, **43**, 3898 (1965).
- [37] L. Xu, P. Kumar, S. V. Buldyrev, S.-H. Chen, P. H. Poole, F. Sciortino, and H. E. Stanley, Relation between the Widom line and the dynamic crossover in systems with a liquid-liquid phase transition, *Proc. Nat. Acad. Sci. USA*, **102**, 16558 (2005).
- [38] J. P. Garrahan, Transition in coupled replicas may not imply a finite-temperature ideal glass transition in glass-forming systems, *Phys. Rev. E*, **89**, 030301 (2014).
- [39] S. Chakrabarty, S. Karmakar, and C. Dasgupta, Phase diagram of glass forming liquids with randomly pinned particles, *arXiv:1404.2701*.
- [40] S. K. Nandi, G. Biroli, J.-P. Bouchaud, K. Miyazaki, and D. R. Reichman, Critical dynamical heterogeneities close to continuous second-order glass transitions. *Phys. Rev. Lett.*, **113**, 245701 (2014).
- [41] G. Biroli, C. Cammarota, G. Tarjus, and M. Tarzia, Random-field-like criticality in glass-forming liquids, *Phys. Rev. Lett.*, **112**, 175701 (2014).
- [42] K. Hukushima and K. Nemoto, Exchange Monte Carlo method and application to spin glass simulations, *J. Phys. Soc. Japan*, **65**, 1604 (1996).
- [43] L. Berthier and W. Kob, The Monte Carlo dynamics of a binary Lennard-Jones glass-forming mixture, *J. Phys.: Condens. Matter*, **19**, 205130 (2007).
- [44] B. Coluzzi, G. Parisi, and P. Verrocchio, Lennard-Jones binary mixture: A thermodynamical approach to glass transition, *J. Chem. Phys.*, **112**, 2933 (2000).
- [45] J. Nocedal and S.J. Wright, *Numerical optimization*, (Springer Verlag, Berlin, 1999).

## Supplementary Information

### I. REPLICA EXCHANGE METHOD

Here we describe the details of the replica exchange method which we have employed in this study, which is basically the repetition of the description in Ref. [1] and in its supplemental information. We have used the parallel tempering algorithm [2, 3] using up to 24 replicas. In this approach, one simulates simultaneously several copies of the system *i.e.*, the same Hamiltonian but each replica is at a different temperature. Using a Boltzmann criterion and the detailed balance condition, we periodically attempt to interchange the configurations of two replicas at different temperatures. Hence each replica makes a random walk in the temperature space. Due to the fast relaxation at high  $T$ , this will lead to an efficient relaxation of the system also at low  $T$ . The smallest difference in temperature between the two neighboring replicas was  $\Delta T = 0.009$ , which guarantees a good overlap of the two potential energy distributions. Attempts to switch the two neighboring replicas have been made every 50000 time steps. We have checked that each parallel tempering run has indeed reached equilibrium by following any given replica and making sure that all tem-



peratures have been sampled sufficiently. A typical path of a replica in temperature space is shown in Fig. SI-5(a). The parallel tempering algorithm indeed allows for the system to be equilibrated down to  $T = 0.44$  even when the concentration of pinned particles,  $c$ , is large. This can be recognized from Fig. SI-5(b), where we show the mean squared displacement (MSD) of the particles (distinguishing the type  $A$  and  $B$  particles) as a function of time. The figure shows that at sufficiently long times the MSD becomes very large, indicating that the particles do indeed move through the box also at high values of  $c$ , even if their relative arrangement does not change much, *i.e.*, one is in the glass state. To calculate physical quantities, we have followed a given replica in the temperature space and considered only the time intervals at which this replica was at the target temperature.

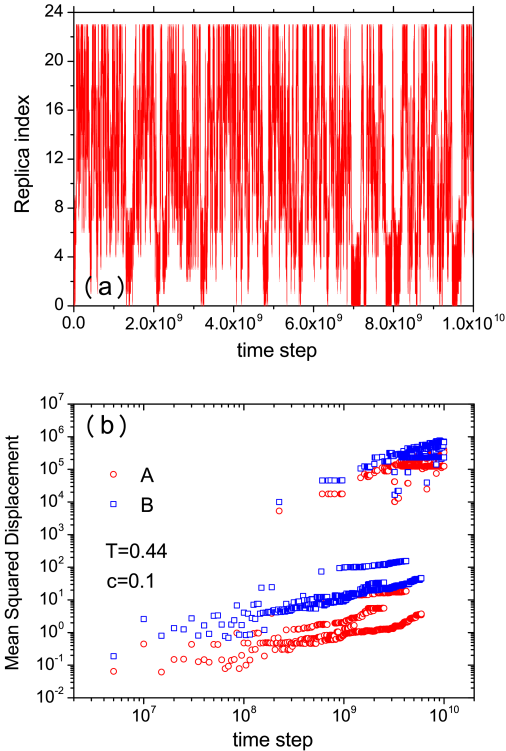


FIG. 5: (a): Time dependence of the trajectory of a typical replica in temperature space for  $T = 0.44$ ,  $c = 0.1$ . (b): The mean squared displacement of  $A$  and  $B$  particles for  $T = 0.44$ ,  $c = 0.1$ .

## II. ENTROPY OF THE PINNED SYSTEMS

For our numerical calculation of the entropy, we employed the thermodynamic integration technique. Although this technique is well-known and has long been applied to bulk systems [4–6], its extension to pinned

systems is not trivial. In this section, we summarize the ideas and present the details of our calculation. We follow the notations introduced in the Method and Materials section.

### A. Definitions

Our starting system is a binary mixture of type  $A$  and  $B$  particles. Since we consider a random pinning of this system, our system is now composed of four different types of particles:  $cN_A$  pinned particles of type  $A$ ,  $cN_B$  pinned particles of type  $B$ ,  $M_A = (1 - c)N_A$  unpinned particles of type  $A$ , and  $M_B = (1 - c)N_B$  unpinned particles of type  $B$ . The total pinned and unpinned particle numbers are  $cN = cN_A + cN_B$  and  $M = M_A + M_B$ , respectively. We denote the coordinate of pinned particles by  $\mathbf{S} = (\mathbf{s}_1, \dots, \mathbf{s}_{cN})$  and unpinned particles by  $\mathbf{R} = (\mathbf{r}_1, \dots, \mathbf{r}_M)$ .

First we consider the thermodynamics of the system with a given configuration of pinned particles  $\mathbf{S}$ . In this situation, the partition function is defined as

$$\tilde{Z}(\mathbf{S}, \beta) = \frac{1}{\Lambda^{3M} M_A! M_B!} \int d\mathbf{R} \exp[-\beta U]. \quad (1)$$

and the thermal average of any variable is

$$\langle A \rangle_{\mathbf{S}, \beta} \equiv \frac{1}{\tilde{Z}(\mathbf{S}, \beta) \Lambda^{3M} M_A! M_B!} \int d\mathbf{R} A \exp[-\beta U], \quad (2)$$

where  $\Lambda$  is the thermal de Broglie wavelength,  $U$  the potential energy, and  $\beta = 1/k_B T$  characterizes the temperature of the system. The free energy and the entropy are now written as

$$\tilde{F}(\mathbf{S}, \beta) = -\frac{1}{\beta} \log \tilde{Z}(\mathbf{S}, \beta), \quad (3)$$

$$\tilde{S}(\mathbf{S}, \beta) = \beta \langle H \rangle_{\mathbf{S}, \beta} - \beta \tilde{F}(\mathbf{S}, \beta), \quad (4)$$

where  $H$  is the Hamiltonian of the unpinned particles.

In this work, we generate pinned particles configurations by fixing a fraction  $c$  particles in the equilibrium configurations, and study the thermodynamics after the disorder average over the realizations of pinned particles. When the pinned particles are generated at a temperature  $\beta'$ , their distribution function is given by

$$P_{\text{pin}}(\mathbf{S}, \beta') = \frac{1}{Z(\beta') \Lambda^{3N} N_A! N_B!} \int d\mathbf{R} \exp[-\beta' U], \quad (5)$$

where  $Z(\beta')$  is the partition function of the bulk system at the temperature  $\beta'$ . Accordingly the thermodynamic quantities to be calculated are given by

$$[\langle A \rangle_{\mathbf{S}, \beta}]_{\beta'} \equiv \int d\mathbf{S} P_{\text{pin}}(\mathbf{S}, \beta') \langle A \rangle_{\mathbf{S}, \beta}. \quad (6)$$

The subscript  $\beta$  of the thermal average  $\langle \dots \rangle$  indicates that the thermal average for unpinned particles are taken at  $\beta$ , while the subscript  $\beta'$  of the disorder average  $[\dots]$  indicates that the pinned particles configurations are obtained from the equilibrium configurations at the temperature  $\beta'$ . Because we are interested mainly in the case  $\beta = \beta'$ , the free energy and the entropy of the system is now written as

$$F(c, \beta) = [\tilde{F}(\mathbf{S}, \beta)]_\beta, \quad S(c, \beta) = [\tilde{S}(\mathbf{S}, \beta)]_\beta. \quad (7)$$

Note that when  $\beta = \beta'$ , the thermodynamic average of a mechanical variable  $A$  becomes exactly

$$[\langle A \rangle_{\mathbf{S}, \beta}]_\beta = \frac{1}{Z(\beta) \Lambda^{3N} N_A! N_B!} \int d\mathbf{S} d\mathbf{R} A \exp[-\beta U], \quad (8)$$

which is nothing but the thermodynamic average for the bulk system at the temperature  $\beta$ . This equivalence is the well-known fact for this type of the pinned system [7].

## B. The thermodynamic integration

### Formulation

To calculate the entropy  $S(c, \beta)$  from simulations, we employ the thermodynamic integration (TI) method. The TI method that is most frequently applied to Lennard-Jones particles is to connect the ideal gas state and the state of interest by a combination of a compression path (increasing density) and a cooling path (decreasing temperature) [4, 5]. However for pinned fluids, it is not clear how compression should be defined. Therefore we use only the cooling path from the ideal gas limit  $T = \infty$  to the target temperature without changing the density. This version of the TI has been used for bulk Lennard-Jones particles [6], and here we apply it to the pinned system.

We first apply the TI to the entropy of a given pinned particles configuration, and then take the disorder average over realizations. The entropy of the system with the pinned particles  $\mathbf{S}$  at the target temperature  $\beta^*$  can be expressed as

$$\tilde{S}(\mathbf{S}, \beta^*) = \tilde{S}(\mathbf{S}, 0) + \beta^* \langle U \rangle_{\mathbf{S}, \beta^*} - \int_0^{\beta^*} d\beta \langle U \rangle_{\mathbf{S}, \beta}. \quad (9)$$

$\tilde{S}(\mathbf{S}, 0)$  is the entropy of  $M$  unpinned particles at  $\beta = 0$ . Since the interactions between the particles including pinned and unpinned particles become irrelevant if  $\beta = 0$ , this term is nothing else than the ideal gas entropy of bulk  $M$  particles. The thermal average of the potential energy can be decomposed as

$$\langle U \rangle_{\mathbf{S}, \beta} = \langle U_{\text{up}} \rangle_{\mathbf{S}, \beta} + U_{\text{p}}(\mathbf{S}) + \langle U_{\text{int}} \rangle_{\mathbf{S}, \beta}, \quad (10)$$

where  $U_{\text{up}}$ ,  $U_{\text{p}}$ , and  $U_{\text{int}}$  are the potential energies of unpinned particles, pinned particles and the interaction between pinned and unpinned particles, respectively. Here we use the fact that  $U_{\text{p}}$  is solely dependent on the configuration of pinned particles and free from the thermal average of unpinned particles. Plugging these into Eq. (9) and taking the disorder average over realizations, we get the final expression

$$\begin{aligned} S(c, \beta^*) = & M \left( 1 - \log \frac{M}{V} \right) - M_A \log \frac{M_A}{M} \\ & - M_B \log \frac{M_B}{M} - 3M \log \Lambda + \frac{3M}{2} \\ & + \beta^* [\langle U_{\text{up}} \rangle_{\mathbf{S}, \beta^*} + \langle U_{\text{int}} \rangle_{\mathbf{S}, \beta^*}]_{\beta^*} \\ & - \int_0^{\beta^*} d\beta [\langle U_{\text{up}} \rangle_{\mathbf{S}, \beta} + \langle U_{\text{int}} \rangle_{\mathbf{S}, \beta}]_{\beta^*}. \end{aligned} \quad (11)$$

In the integral, the temperature for the thermal average runs from  $\beta = 0$  to  $\beta = \beta^*$ , while the temperature for the disorder average over realizations of the pinned particles is fixed to be the target temperature  $\beta^*$ . Thus we cannot use the relation Eq. (8) to evaluate the integrands. Instead we need to directly calculate the potential energy at  $\beta \in [0, \beta^*]$  under a given pinned particles configuration  $\mathbf{S}$  and take the disorder average over realizations.

### Implementation

The integral in Eq. (11) is decomposed into three temperature regimes and each of them is evaluated separately. (1) For low temperature regime, we calculate the potential energy from the configurations generated by the parallel tempering calculations outlined in Sec. I. From each trajectory, we obtain the thermal average of the potential energies  $U_{\text{up}}$  and  $U_{\text{int}}$  at different temperatures with a given pinned particles configuration. We employ the Simpson's rule to evaluate the integral and take the disorder average over realizations. (2) Above the highest temperature in the parallel tempering calculations, we use standard Monte Carlo method to calculate the potential energy. We slice the temperature into the grids with the width  $\Delta\beta = 0.001 - 0.01$  depending on the temperature range and calculate the thermal average of  $U_{\text{up}}$  and  $U_{\text{int}}$  at each temperature for a given pinning configuration. We employ the Simpson's rule to evaluate the integral and take the disorder average over realizations. (3) We take a special care about the integration at very high temperature  $\beta < 0.001$ , since the potential energies  $U_{\text{up}}$  and  $U_{\text{int}}$  diverge in the high temperature limit. To accurately calculate the integral, we first fit the potential energy data to a polynomial function then analytically integrate the function. Considerations on the high temperature expansion shows that the potential energy of the Lennard-Jones particles at high temperature behaves as

$$\langle U \rangle = A\beta^{-1/4} + B\beta^{-1/2} + C\beta^{-3/4} + \mathcal{O}(1), \quad (12)$$

where  $A$ ,  $B$  and  $C$  are constants [6]. We thus fit the data of  $\langle U_{\text{up}} \rangle_{\mathbf{S},\beta} + \langle U_{\text{int}} \rangle_{\mathbf{S},\beta}$  with expression (12) to obtain these constants and integrate it analytically. In Fig. SI-6, we show the raw data of  $\beta^{3/4}(\langle U_{\text{up}} \rangle_{\mathbf{S},\beta} + \langle U_{\text{int}} \rangle_{\mathbf{S},\beta})/M$  and the fitting function Eq. (12) as a function of  $\beta^{1/4}$ , confirming that Eq. (12) holds well.

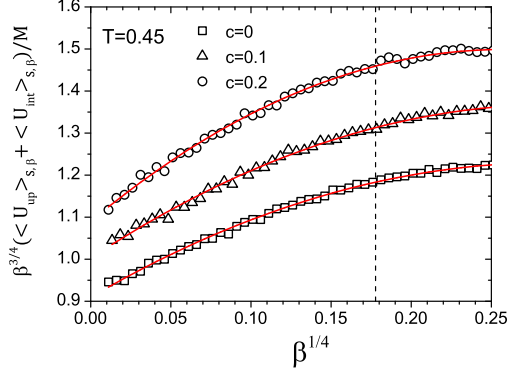


FIG. 6:  $\beta^{3/4}(\langle U_{\text{up}} \rangle_{\mathbf{S},\beta} + \langle U_{\text{int}} \rangle_{\mathbf{S},\beta})/M$  as a function of  $\beta^{1/4}$  for very high  $T$  ( $> 250$ ). The raw data (symbols) are fitted well by the fitting curves (red solid lines). The vertical dashed line indicates the temperature above which we use the analytical integration. Note that we show here only the data for one realization of the pinned particles since the curves will depend on the realization.

### C. Vibrational entropy

We next summarize the method to calculate the harmonic vibrational entropy of the pinned system. We consider the system that weakly vibrates around an inherent structure (IS). If we denote by  $\delta \mathbf{r}_i$  the displacement of the  $i$ -th particle from its position in the inherent structure, the potential energy can be approximated well as

$$U \approx U_{\text{IS}}(\mathbf{S}) + \frac{1}{2} \sum_{i,j}^M \frac{\partial^2 U}{\partial \mathbf{r}_i \partial \mathbf{r}_j} \delta \mathbf{r}_i \delta \mathbf{r}_j. \quad (13)$$

It is important to realize that only the derivative of the potential energy respect to the coordinates of unpinned particles should be taken into account, not including the ones of pinned particles (But of course  $U$  will depend on the positions of the pinned and unpinned particles). Thus the size of the Hessian matrix is  $(3M \times 3M)$ . Introducing the eigenvalues  $\lambda_1, \dots, \lambda_{3M}$  of the Hessian, the harmonic vibrational entropy of the given inherent structure with a given pinned particle configuration can be written as

$$\tilde{S}_{\text{IS,vib}}(\mathbf{S}, \beta) = \sum_{a=1}^{3M} \left\{ 1 - \log(\beta \hbar \sqrt{\lambda_a/m}) \right\}. \quad (14)$$

Note that the eigenvalues  $\lambda_a$  depends on the choice of the inherent structure and the pinned particle configuration. Taking the average of  $\tilde{S}_{\text{IS,vib}}(\mathbf{S}, \beta)$  over realizations of pinned particle configurations and the inherent structures, we finally obtain the harmonic vibrational entropy of pinned system  $S_{\text{vib}}(c, \beta)$ .

In practice, we have sampled the inherent structure by minimizing the potential energy of instantaneous configurations obtained in the simulations. For this calculation we used the conjugate-gradient method. Note that the pinned particles were frozen during the minimization process and only the coordinates of the unpinned particles are optimized.

### D. Finite size effect

In Fig. SI-7, we show  $S_c$  for  $N = 150$  and  $300$  for several state points. We find that finite size effects are small, at least for these two system sizes.

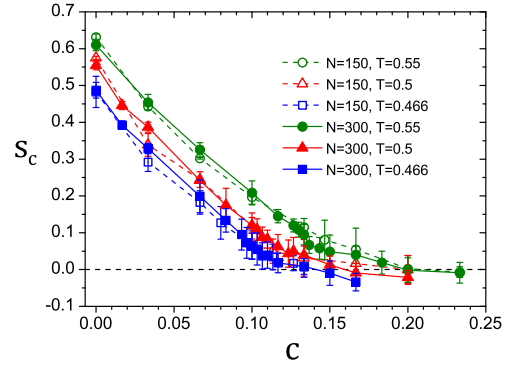


FIG. 7: Finite size effect of the configurational entropy for  $N = 150$  and  $N = 300$ .

## III. OBTAINING THE KAUZMANN TEMPERATURE FROM THE OVERLAP

We have determined the averaged distribution function  $[P(q)]$  of the overlap  $q$  as explained in the main text. Subsequently we have calculated the skewness  $\gamma(c, T)$  as

$$\gamma = \frac{\int_0^1 dq [P(q)] (q - [\langle q \rangle])^3}{\left( \int_0^1 dq [P(q)] (q - [\langle q \rangle])^2 \right)^{3/2}}. \quad (15)$$

The  $T$ - and  $c$ -dependence of  $\gamma$  is shown in Fig. SI-8. The point at which  $\gamma$  is zero is used to define the Kauzmann temperature  $T_K^{(q)}$  shown in Fig. 4 of the main text.

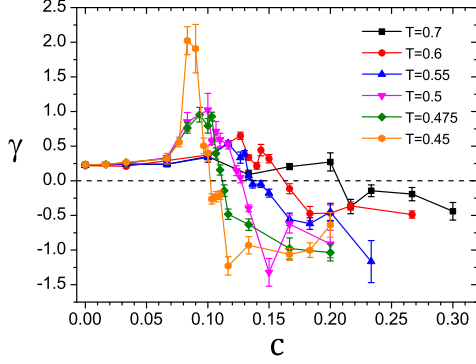


FIG. 8: The skewness  $\gamma$  of the distribution function  $[P(q)]$ . The horizontal dashed line is the zero-axis and used to define  $T_K^{(q)}$ . The error bars have been calculated using the jackknife method.

#### IV. SADDLE POINTS AND DYNAMIC TRANSITION POINT

In Fig. SI-9(a), we show the original data of Fig. 3(b) of the main text. This scatter plot shows the normalized saddles index  $k$  as a function of the energy at the saddle,  $e_{\text{SP}}$ , obtained from the minimization of the square gradient potential  $W = \frac{1}{2}|\nabla U|^2$  [8, 9]. Fig. 3(b) in the main text has been obtained by averaging over this scatter data for a given  $e_{\text{SP}}$ . The threshold energy  $e_{\text{th}}$  is extracted from Fig. 3(b) of the main text as a point at which the averaged  $k$  vanishes. Mapping of  $e_{\text{th}}(c)$  to the dynamic transition temperature  $T_d(c)$  can be done by plotting the temperature dependence of the inherent structures  $[\langle e_{\text{IS}} \rangle]$ . The reason why we use the inherent structures  $[\langle e_{\text{IS}} \rangle]$  instead of  $[\langle e_{\text{SP}} \rangle]$  is that in practice one can evaluate the  $T$ -dependence of  $[\langle e_{\text{IS}} \rangle]$  with higher precision than that of  $[\langle e_{\text{SP}} \rangle]$ . Note that using  $[\langle e_{\text{SP}} \rangle]$  would in fact give the same result since it is expected to be very close to  $[\langle e_{\text{IS}} \rangle]$  in the low temperature regime. In Fig. SI-9(b) we show the  $T$ -dependence of  $[\langle e_{\text{IS}} \rangle]$  for several  $c$ 's. The inherent structures are found to be a monotonic function of  $T$  for all  $c$ 's and therefore  $e_{\text{th}}$  can be uniquely mapped to  $T_d$ .

#### V. DYNAMIC TRANSITION TEMPERATURES

The dynamic transition temperatures  $T_d$  can be evaluated by two methods: the dynamic route and the static one [8–10]. In the dynamic route,  $T_d$  is obtained directly by fitting the relaxation time  $\tau_\alpha$  from the time-dependent correlation functions, such as the scattering function  $F_s^A(k, t)$ , to the MCT power-law  $\tau_\alpha \propto |T - T_d^{(\text{fit})}|^{-\gamma}$ . Thus in this case one has  $T_d^{(\text{fit})}$ ,  $\gamma$ , and the prefactor are fit parameters, all of which will depend on  $c$ . In the present paper, we have adopted the alternative static

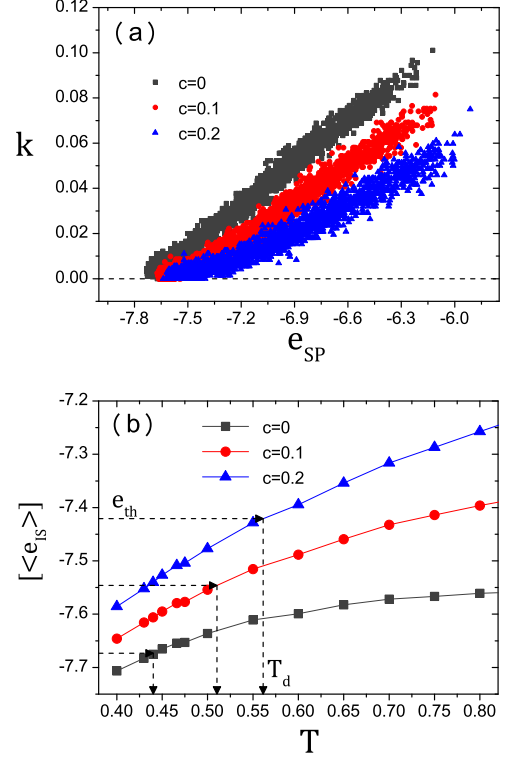


FIG. 9: (a): The scatter plot of  $k$  vs  $e_{\text{SP}}$ . (b): The  $[\langle e_{\text{IS}} \rangle]$  as a function of  $T$ . The horizontal and vertical arrows indicate the location of  $e_{\text{th}}(c)$  and  $T_d(c)$ , respectively. This plot is used to map  $e_{\text{th}}(c)$  to  $T_d(c)$ .

route to obtain  $T_d$  defined as a point at which the saddles of the potential energy landscape vanish. For bulk systems,  $c = 0$ , it has been found that  $T_d^{(\text{fit})}$  from fitting (dynamic) agrees very well with  $T_d$  as determined from the saddles (static) [8, 9].

We follow exactly the same method to obtain  $T_d^{(\text{fit})}$  for the pinned systems, i.e.  $c \neq 0$ . In Fig. SI-6(a), we plot  $\tau_\alpha$  obtained from  $F_s^A(k, t)$  as a function of  $T - T_d^{(\text{fit})}$  for several values of  $c$ . Both  $T_d^{(\text{fit})}$  and  $\gamma$  are used as fitting parameters to obtain the good fit with the power-law. As it is well known for bulk systems, special care has to be taken to choose an optimized temperature windows over which  $\tau_\alpha$  can be fitted by a power-law and we have thus put the emphasis to get a good fit in the low temperature part of the data.

In Fig. SI-6(b) we plot the so obtained  $T_d^{(\text{fit})}$  in the phase diagram presented in the main text. It is clear that the agreement of the two dynamic transition temperatures obtained from different routes is very good. However, we also recognize that the  $c$ -dependence of  $T_d^{(\text{fit})}$  is noisier. This is most likely due to the subtleties of the fitting procedures since three free fit parameters have to be used for  $T_d^{(\text{fit})}$  ( $T_d^{(\text{fit})}$ ,  $\gamma$ , and prefactor), whereas no



fitting parameter is required to evaluate  $T_d$  from the saddles. This is the reason why in the present study we put more emphasis on the static method.

## VI. VIOLATION OF THE ADAM-GIBBS RELATION

In this section we will show that for the pinned fluid the Adam-Gibbs relation  $\ln \tau_\alpha \propto 1/Ts_c$  [11, 12] is violated. In Fig. SI-7, we plot the relaxation time  $\tau_\alpha$  against  $1/Ts_c$  for different values of  $c$ . For  $c = 0$ , one observes that  $\ln \tau_\alpha$  is indeed a linear function of  $1/Ts_c$  and that therefore the AG relation holds, as it has been already documented in Refs.[13, 14]. However, as  $c$  increases,  $\log \tau_\alpha$  systematically deviates from the linear dependence and becomes a convex function of  $1/Ts_c$ . Thus this result clearly demonstrates the violation of the AG relation for pinned fluids.

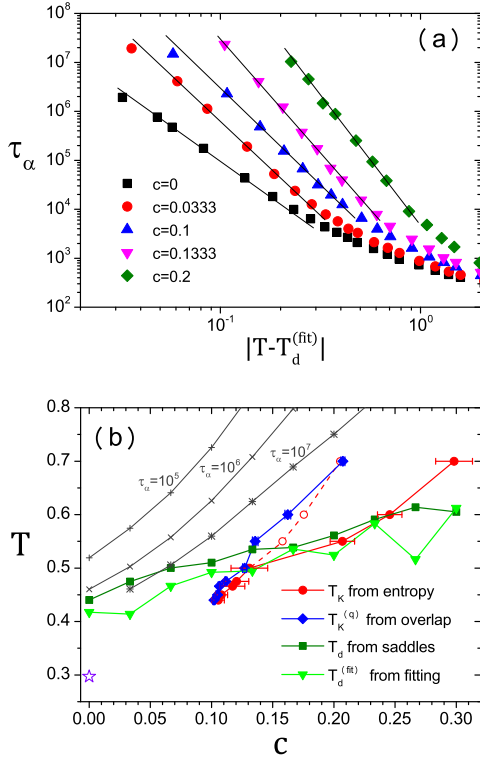


FIG. 10: (a): Test of the validity of the MCT power-law fit to  $\tau_\alpha$  where  $T_d^{(fit)}$  is a fitting parameter. The solid lines indicate the MCT power-law. (b): Phase diagram including the  $T_d^{(fit)}$ (c) line.

[1] W. Kob and L. Berthier, Probing a Liquid to Glass Transition in Equilibrium, *Phys. Rev. Lett.*, **110**, 245702

(2013).  
[2] K. Hukushima and K. Nemoto, Exchange Monte Carlo

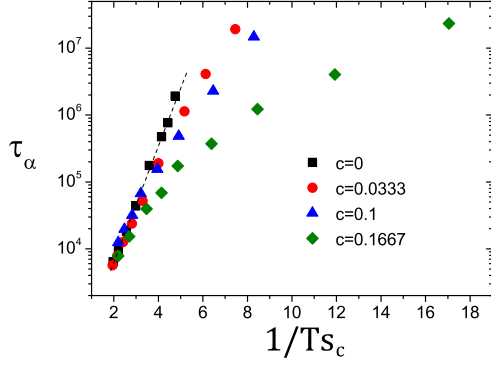


FIG. 11: Logarithm of the relaxation time as a function of  $1/Ts_c$ . Within the Adam-Gibbs theory one expects that this representation of the data gives rise to a linear dependence, which for  $c > 0$  is evidently not the case.

Method and Application to Spin Glass Simulations, *J. Phys. Soc. Japan*, **65**, 1604 (1996).

- [3] R. Yamamoto and W. Kob, Replica-exchange molecular dynamics simulation for supercooled liquids, *Phys. Rev. E*, **61**, 5473 (2000).
- [4] F. Sciortino, W. Kob, and P. Tartaglia, Inherent Structure Entropy of Supercooled Liquids, *Phys. Rev. Lett.*, **83**, 3214 (1999).
- [5] S. Sastry, Evaluation of the configurational entropy of a model liquid from computer simulations, *J. Phys: Condensed Matt.*, **12**, 6515 (2000).
- [6] B. Coluzzi, G. Parisi, and P. Verrocchio, Lennard-Jones binary mixture: A thermodynamical approach to glass transition, *J. Chem. Phys.*, **112**, 2933 (2000).
- [7] P. Scheidler, W. Kob, and K. Binder, The Relaxation Dynamics of a Supercooled Liquid Confined by Rough Walls, *J. Phys. Chem. B*, **108**, 6673 (2004).
- [8] L. Angelani, R. Di Leonardo, G. Ruocco, A. Scala, and F. Sciortino, Saddles in the Energy Landscape Probed by Supercooled Liquids, *Phys. Rev. Lett.*, **85**, 5356 (2000).
- [9] K. Broderix, K. K. Bhattacharya, A. Cavagna, A. Zippelius, and I. Giardina, Energy landscape of a Lennard-Jones liquid: Statistics of stationary points, *Phys. Rev. Lett.*, **85**, 5360 (2000).
- [10] W. Götze, "Complex Dynamics of Glass-Forming Liquids", (Oxford University Press, Oxford, 2009).
- [11] G. Adam and J. H. Gibbs, On the Temperature Dependence of Cooperative Relaxation Properties in Glass-Forming Liquids, *J. Chem. Phys.*, **43**, 139 (1965).
- [12] G. Biroli and J.-P. Bouchaud, The random first-order transition theory of glasses: a critical assessment, In P. G. Wolynes and V. Lubchenko, Eds., *Structural Glasses and Supercooled Liquids: Theory, Experiment, and Applications* (Wiley, New York, 2012).
- [13] A. Scala, F. W. Starr, E. La Nave, F. Sciortino, and H. E. Stanley, Configurational entropy and diffusivity of supercooled water, *Nature*, **406**, 166 (2000).
- [14] S. Sastry, The relationship between fragility, configurational entropy and the potential energy landscape of glass-forming liquids, *Nature*, **409**, 164 (2001).